Dynamics of the global meridional ice flow of Europa's icy shell

Yosef Ashkenazy [1]*, Roiy Sayag[1] and Eli Tziperman [2]

Europa is one of the most probable places in the solar system to find extra-terrestrial life[1,2], motivating the study of its deep (~100 km) ocean[3-6] and thick icy shell[3,7-11]. The chaotic terrain patterns on Europa's surface[12-15] have been associated with vertical convective motions within the ice[8,10]. Horizontal gradients of ice thickness[16,17] are expected due to the large equator-to-pole gradient of surface temperature and can drive a global horizontal ice flow, yet such a flow and its observable implications have not been studied. We present a global ice flow model for Europa composed of warm, soft ice flowing beneath a cold brittle rigid ice crust[3]. The model is coupled to an underlying (diffusive) ocean and includes the effect of tidal heating and convection within the ice. We show that Europa's ice can flow meridionally due to pressure gradients associated with equator-to-pole ice thickness differences, which can be up to a few km and can be reduced both by ice flow and due to ocean heat transport. The ice thickness and meridional flow direction depend on whether the ice convects or not; multiple (convecting and non-convecting) equilibria are found. Measurements of the ice thickness and surface temperature from future Europa missions[18,19] can be used with our model to deduce whether Europa's icy shell convects and to constrain the effectiveness of ocean heat transport.

The surface properties of Europa and its tidal forcing are well known, yet its inner structure and properties are less certain[7,12]. The known surface properties include the incoming solar radiation[16] (~16 W m^{-2} year-round at the equator and between 0 and ~4 W m^{-2} at the poles) and the tidal forcing that is expected to lead to a triaxial ellipsoid structure[17] at a period of 3.55 Earth days[16]. Among the less certain interior properties are the thickness of the outer ice layer[20,21] (estimated as a few km to more than 30 km), depth of the subsurface ocean[3] (~100 km), and rates of heating at the ocean bottom due to tidal heating within the core[22] (33–230 mW m^{-2}) and of radiogenic heating (~8 mW m^{-2}) due to the assumed chondritic abundance of U, K and Th in the solid iron core[23] (oceanic tidal heating is negligible[22]). Our focus here is the global-scale horizontal ice flow on Europa. The polar surface of Europa is colder by tens of degrees than the equatorial regions[16,24], which could lead to meridional ice thickness gradients and therefore to pressure gradients that may drive ice flow from high to low latitudes. This is reminiscent of Snowball Earth events over 580 million years ago, when the ocean was covered by a ~1-km-thick ice layer[25]. Ice tidal movements result in a strain rate and heating within the ice that varies in both the zonal and meridional directions[16,17] and can also lead to a large-scale lateral ice flow.

Europa's ice thickness is significantly smaller than the horizontal scales of global ice flow, justifying the use of the 'shallow ice approximation', which is commonly used to represent soft land ice flow over the solid Earth surface[26]. Our two-dimensional (latitude-depth) ice flow model for Europa is therefore based on an 'upside-down' shallow ice approximation, representing soft, flowing ice under a cold rigid external ice crust[3], separated by a ductile-to-brittle transition zone. The model is coupled with a simple (one layer) ocean model whose meridional heat transport is parameterized via effective diffusivity, which is meant to represent the transport by both ocean circulation and eddies. The model's variables are the ice flux q, ice thickness h_1, and ocean temperature T_o and salinity S_o (see Methods). The model includes the role of geothermal heating at the ocean bottom and the ice-tidal heating, and parameterizes vertical convection within the ice. The annual mean surface temperature, T_s, is calculated based on the energy balance between the incoming solar radiation, internal heating and outgoing longwave radiation[16].

Below, we first show that when the roles of ocean and ice convection are ignored the ice flow effectively homogenizes observable horizontal ice thickness gradients. We then show that meridional ocean heat transport can lead to the homogenization of ice thickness as well. Finally, we show that ice convection can lead to reversed equator-to-pole ice flow in which the enhanced polar tidal heating plays a major role.

Starting with the simplest case, Fig. 1 shows the model's equilibrium solution when taking into account the tidal heating, but disabling ice convection and meridional ocean heat transport, such that the heat flux into the ice base is locally equal to the geothermal heating rate at the ocean bottom, $Q_g = 0.05$ W m^{-2} (ref. [22]). Given the uncertainties in grain size, and therefore ice viscosity[27], we calculated the model's solution for a range of melting viscosity values, η_0.

Figure 1b shows that the ice is thicker at the poles, where the surface temperature is colder. It also shows that a global pole-to-equator ice flow develops (Fig. 1d,f). The equator-to-pole thickness difference is dramatically reduced when ice flow is present for the lower values of the specified melting viscosity, from 3.2 km for the stiffer ice to only 350 m for the softer ice. The maximum meridional ice flux occurs where thickness gradients are maximal (Fig. 1d), and the ice velocity is maximal at the bottom of the ice where it is softest and decreases rapidly upward as the ice becomes stiffer. The ice stiffness is exponential in terms of ice temperature, which (Fig. 1c) varies nearly linearly with depth in this case, not being affected by the presence of weak ice tidal heating. Smaller viscosity also leads to smaller mean ice thickness because the softer ice allows for more tidal heating within the ice (see equation (11); ref. [9]). The freezing at high latitudes and melting at low latitudes imply an equatorward flow (Fig. 1e). The maximal melting in the cases corresponding to mid-range and softer ice viscosity (blue and red curves) is at mid-latitude due to the value of the vertical temperature gradient at the ice bottom as a function of latitude (see equation (9)).

---

[1]Department of Solar Energy and Environmental Physics, The Jacob Blaustein Institutes for Desert Research, Ben-Gurion University of the Negev, Midreshet Ben-Gurion, Israel. [2]Department of Earth and Planetary Sciences and School of Engineering and Applied Sciences, Harvard University, Cambridge, MA, USA. *e-mail: ashkena@bgu.ac.il
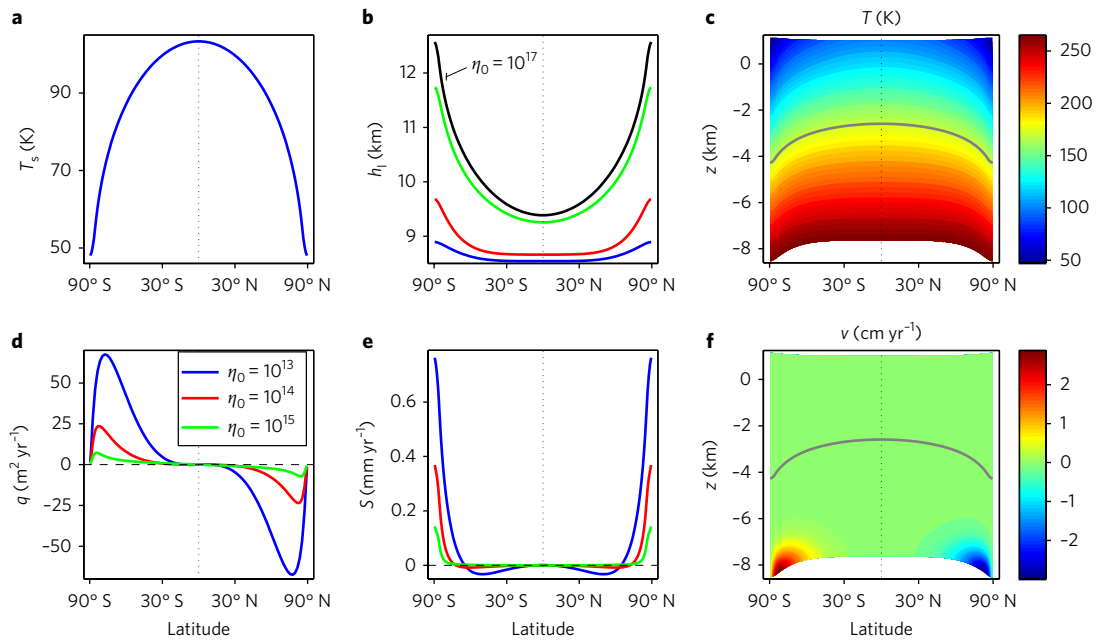
Fig. 1 | Equilibrium state of the icy shell of Europa when the meridional ocean heat transport and ice convection are not included. a–f, We show the meridional (latitudinal) distribution of surface ice temperature (**a**), ice thickness (**b**), meridional ice transport (**d**) and ice freezing rate (**e**), for several melting viscosities ($\eta_0 = 10^{13}$, 10^{14} and 10^{15} Pa·s), as well as the ice temperature (**c**) and meridional ice velocity (**f**) as a function of vertical coordinate and latitude for $\eta_0 = 10^{14}$ Pa·s. As the ice floats over the ocean, sea level is denoted here as $z = 0$, where the ice level below sea level is $z_b = -\mu h_i$ and the thickness above sea level is $z_s = (1 - \mu)h_i$. The grey lines in **c** and **f** indicate the depth of the ductile-to-brittle transition.

The effective homogenization of ice thickness by the global flow is large enough to be detected by the future missions to Europa.

We now proceed to the second case, which includes oceanic heat transport, but no ice convection (Fig. 2). The ocean heat transport is represented as a diffusive process with an eddy coefficient κ_o that is varied over several orders of magnitude. This simplified representation allows us to study the effect of a very broad range of heat transport efficiencies due to both ocean circulation and eddies[25,28–30]. When the ocean efficiently transports heat (a larger eddy coefficient), the gradients in ice thickness are much smaller than in the case of an ocean that does not transport heat efficiently (Fig. 2a): in the absence of ocean heat transport, melting occurs at low latitudes because the geothermal heat flux that is transferred directly from

the ocean bottom into the ice base is larger than the upward diffusive heat flux within the ice (equation (9)) and this heat excess leads to melting. Freezing at high latitudes[11] occurs due to the opposite situation. The ocean heat transport carries the heat excess at low latitudes to high latitudes, such that the heat flux from the ocean into the ice base nearly balances the upward diffusive heat flux within the ice at all latitudes. The resulting lower melting and freezing rates (Supplementary Fig. 1b) eliminate the need for meridional ice transport, which is therefore smaller (Fig. 2b). Smaller meridional thickness gradients imply weaker ice transport. The latitudinal variations in ocean temperature (Fig. 2a, right axis) are very small. The ocean temperature is nearly linear in ice thickness and the two are therefore represented by the same curves in Fig. 2a, mostly because the temperature is close to the freezing temperature (Supplementary Fig. 1a), which in turn is linear in ice thickness due to the dependence of melting temperature on pressure (Methods).

Interestingly, without ocean heat transport (Fig. 1), a smaller equator-to-pole thickness difference (blue curve, $\eta_0 = 10^{13}$ Pa·s) occurs in combination with a strong meridional ice flow, while in the presence of effective ocean heat transport, a small equator-to-pole thickness difference occurs in combination with a weak ice flow (Fig. 2, black curve, $\kappa_o = 1$ m^2 s^{-1}). Finally, the ice thickness, ice flux, ice velocity and melting rates are hardly affected when ocean salinity transport is included. However, previous studies[31] have shown that salinity transport within the ice can significantly influence the partial melting and therefore the ice flow.

When included, the ocean salinity exhibits larger meridional gradients for smaller oceanic eddy mixing coefficients, weakly affecting the freezing rates and ocean temperatures (Supplementary Fig. 2). Estimates of Europa's ocean salinity vary widely, from being nearly fresh to highly saline[32]. We chose an intermediate value of 50 ppt and show the sensitivity to this value in Supplementary Fig. 6.

Previous studies have shown that a sufficiently thick icy shell may convect, creating an upper stagnant conductive layer overlaying a lower vertically convecting one[7,9,17,27,33]. It has been suggested that ice

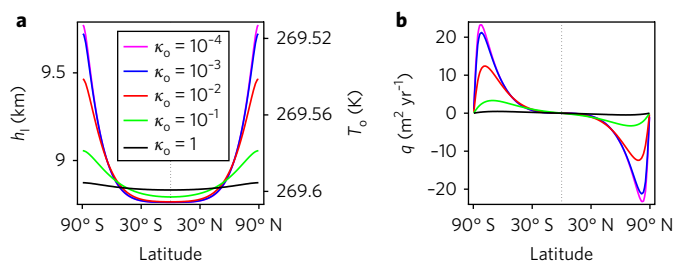**Fig. 2 | Equilibrium state of the icy shell of Europa when ocean heat transport is included, while ice convection is absent. a,b**, We show the ice thickness (**a**) and ice flux (**b**) as a function of latitude. The ocean temperature is linearly related to ice thickness and the corresponding values are presented on the right vertical axis of **a**. The results are shown for several values of the ocean eddy mixing coefficient $\kappa_o = 10^{-4}$, 10^{-3}, 10^{-2}, 10^{-1} and 1 m^2 s^{-1}. Here, the melting viscosity is set to $\eta_0 = 10^{14}$ Pa·s. Smaller meridional gradients are obtained for more efficient ocean heat transport (larger ocean eddy mixing coefficients).

convection enhances tidal heating[9], affects ice transport[17] and leads to multiple solutions under the same forcing (bi-stability) in the solution for the thickness[27]. We therefore examined the effect of ice convection on ice flow and ice thickness in the absence of ocean heat transport (Fig. 3). The ice temperature in the convecting lower layer (Fig. 3c) is much more uniform and closer to the freezing temperature than in the absence of convection (Fig. 1c). The ice is relatively soft in the convective layer, where tidal heating is also larger[9] and extends over a much wider depth range than in the non-convecting case (Fig. 3a). Furthermore, the ice is more than 3 km thicker than in the non-convecting case. When convecting, the ice is composed of a conducting layer (the depth range above the dashed line in Fig. 3c) overlaying a 5–6-km-thick convecting layer. Due to the enhanced high latitude total tidal heating (Fig. 4d), melting increases there and the polar ice becomes thinner than that at low latitudes. Consequently, for not-very-high values of the melting viscosity, the ice flow reverses to be from the equator to the poles (Fig. 3d,f). Moreover, the ice velocity within the deep convective layer is significantly larger (Fig. 3f versus Fig. 1f) and the meridional ice flux is more than 16 times larger than that without convection (Fig. 3d).

Our parameterized convection scheme leads to bi-stability, also found in previous, non-global ice models[27], and the two possible equilibrium solutions for the average ice thickness as a function of the melting viscosity are shown in Fig. 3e. The convective solution is characterized by more uniform thickness, thicker ice and stronger, reversed (equator-to-poles) ice transport (Fig. 3b,d) for $\eta_0 < 6 \times 10^{14}$ Pa·s. We note, though, that previous studies of local convection on Europa suggested that convection generally happens for thicker ice than that found using our simple convection

parameterization at any given viscosity value[7,9,27,34,35] and, in the future, such local calculations could be used as further constraints on the convection parameterization.

The solutions presented here and the above discussion have important observational implications. Instantaneous and daily mean surface temperatures have been estimated by the Galileo mission[24] and are expected to be observed again by the European Space Agency's JUpiter ICy moons Explorer (JUICE) mission[18] and, in particular, by the National Aeronautics and Space Administration's Europa Clipper mission[19], which is also expected to observe the ice thickness. We found that potentially observable weak equator-to-pole thickness gradients may result either from low viscosity leading to stronger meridional ice transport or effective meridional ocean heat transport in conjunction with weak ice transport.

Consider two examples of using observations to deduce aspects of Europa's icy shell and ocean dynamics, demonstrated in Fig. 4 using the model that now includes all elements: ice flow, convection and ocean heat transport. First, Fig. 4a,b shows the equator-to-pole thickness difference (colours) and mean ice thickness (contours) as functions of the melting viscosity and the ocean eddy mixing coefficient for the convecting (Fig. 4a) and non-convecting (Fig. 4b) solutions. Given the observations of the ice thickness and the equator-to-pole ice thickness difference, we can determine whether the ice is convecting and constrain the viscosity and ocean heat transport coefficients. As an example, the black '×' symbol in Fig. 4b marks a thickness of 9.4 km and a thickness difference of 1.25 km. These values imply that the ice is not convecting (such values do not occur in Fig. 4a) and that the two unobservable parameters of melting viscosity and ocean eddy mixing coefficient are constrained
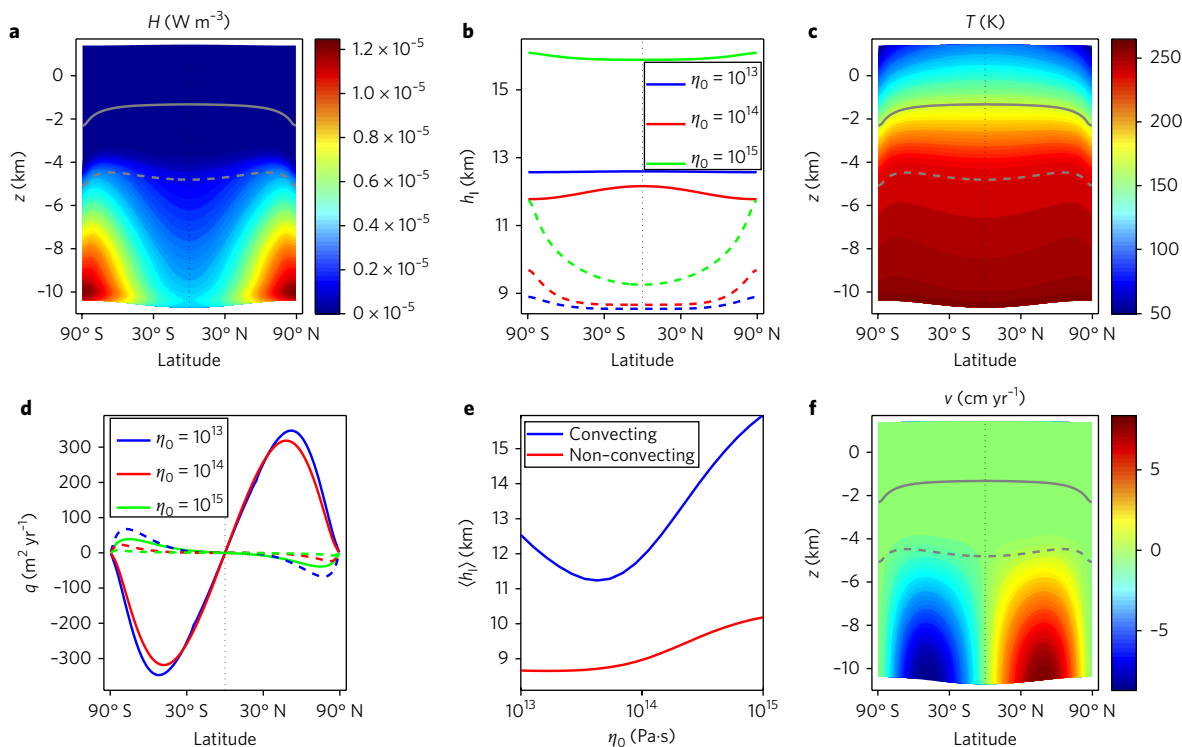

Fig. 3 | Equilibrium solutions when meridional ocean heat transport is absent and ice convection is active. a–f, We show the tidal heating (**a**), ice thickness (**b**), ice temperature (**c**), meridional ice transport (**d**) as a function of latitude, and the mean ice thickness as a function of the melting viscosity coefficient η_0 when the ice is convecting (blue) and non-convecting (red) (**e**) and meridional ice velocity (**f**). In **c** and **f**, the solid grey line indicates the ductile-to-brittle transition depth and the dashed grey line indicates the top of the convecting layer (see Methods). The dashed lines in **b** and **d** indicate the equilibrium states for the non-convecting case also shown in Fig. 1b,d. The melting viscosity is set to $\eta_0 = 10^{14}$ Pa·s in **c** and **f**. Note the dramatic differences between the convecting and non-convecting solutions (**b**, **d** and **e**; see Fig. 1 for comparison).
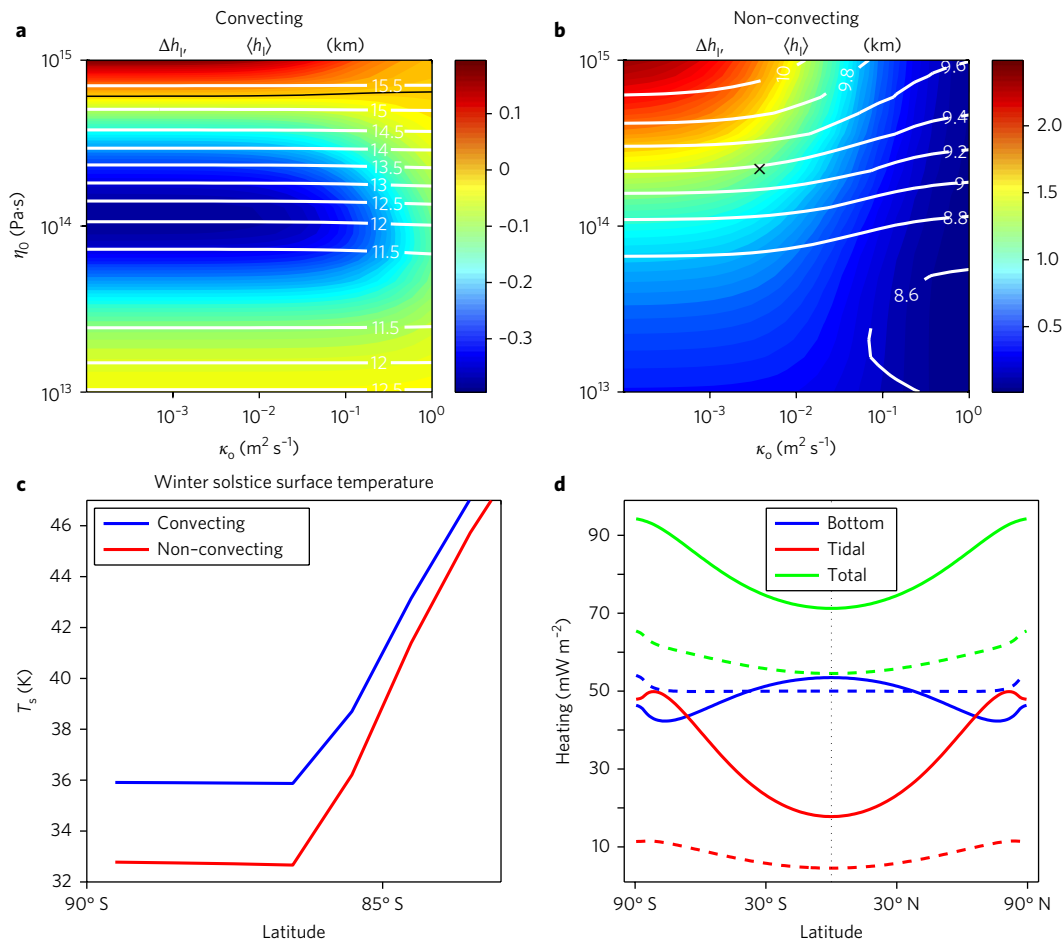
Fig. 4 | Observational predictions and verification. a, Equator-to-pole ice thickness difference (colours) and mean ice thickness (white contours) when the ice is convecting. **b**, Same as **a**, but for non-convecting solutions. Both **a** and **b** are shown as a function of the ocean eddy mixing coefficient, κ_o, and melting viscosity coefficient η_0. The solid black line in **a** indicates the zero ice thickness difference. **c**, Winter solstice high latitude ice surface temperature as a function of latitude when the ice is convecting (blue) and non-convecting (red). **d**, Heat flux at the bottom of the ice (blue), vertically integrated tidal heat flux (red) and total heating (green) when the ice is convecting (solid lines) and non-convecting (dashed lines).

to be $\eta_0 = 2.15 \times 10^{14}$ Pa·s and $\kappa_o = 3 \times 10^{-3}$ m^2 s^{-1}. These estimates are subject to all model assumptions and to the uncertainty in the model parameters. The corresponding minimum and maximum ice fluxes are shown in Supplementary Fig. 3.

Note that in the convective state, the pole-to-equator thickness difference is negative in most parameter domains (below the black contour in Fig. 4a), indicating thicker equatorial ice. Because we include the effect of meridional ice flow here, this testable prediction is quite different from that discussed in ref. [17], where a thicker equator was predicted only for very weak geothermal heating. Nimmo et al.[17] also conjectured the convecting case to be of a nearly uniform thickness due to the homogenization by lateral flow, as confirmed by our results (Fig. 3b, solid lines).

As a second example of observational constraints, consider the winter solstice surface ice temperature at the high latitudes (Fig. 4c), showing a difference of 3.1 K between the convecting and non-convecting solutions. Because of the lack of insolation at the winter pole, the heat flux coming out of the ice is the only heat source and is balanced by longwave radiation, determining the surface temperature. This heat flux is higher in the convecting case due to greater tidal heating (Figs. 3a and 4d). This is a small difference, yet it may be observable.

The model presented here lacks important features, including zonal thickness variations due to tidal effects[9,16,17], the effect of the

tidal strain rate on the non-Newtonian ice rheology[16,27], our use of a simple convection parameterization[7,9,27] and the use of a simplified ocean representation. Previous, more detailed localized convection studies[7,27] suggested that convection occurs for a thicker icy shell than reported here. In addition, there are some unknown or poorly constrained parameters, such as geothermal heat flux, ice melting viscosity and the ocean eddy heat transport coefficient.

While simple, the main qualitative conclusions of our model—that the ice flows under its weight, that this flow weakens as a result of meridional ocean heat transport and that convection plays an important role in the direction and intensity of the ice flow—should be robust. These results may be relevant to future missions such as JUICE[18] and Europa Clipper[19].

Methods

First, we briefly summarize the model equations. Then, we demonstrate the robustness of the results to various aspects of model formulation and provide a detailed description of each of the model components. The parameters are listed in Supplementary Table 1.

Model overview. The ice thickness h_I is governed by a mass conservation equation based on an 'upside-down' shallow ice approximation,

$$\partial_t h_I + \frac{1}{r\sin\theta}\partial_\theta(q\sin\theta) = \frac{1}{\mu}S$$

where θ is the latitude, the meridional ice transport $q(\theta)$ is calculated from the ice thickness gradients, $S(\theta)$ is the source term due to freezing and melting at the base of the ice, r is the radius of Europa and μ is the ratio between ice and water densities.

The ocean temperature T_o and meridional heat flux are determined via a heat budget that incorporates geothermal heat flux from the ocean bottom, Q_g, into the ice base and parameterized eddy heat transport by both ocean macro-turbulence and large-scale circulation,

$$\rho_o c_{p,o} h_o \partial_t T_o = Q_g - \beta(T_o - T_f) + \frac{\rho_o c_{p,o}}{r^2 \sin\theta} \partial_\theta (h_o \kappa_o \sin\theta \partial_\theta T_o)$$

where ρ_o is the reference density for Europa's ocean, $h_o(\theta)$ is the ocean depth and $T_f(\theta)$ is the freezing temperature. Both the ice thickness and ocean temperature are solved from 89° S to 89° N, with a 1/2° resolution. No flow boundary conditions for the meridional velocity ($v = 0$) and no flux conditions for temperature and salinity are applied at the poles. The vertical temperature within the ice is determined by a temperature equation that incorporates tidal heating and a parameterization of vertical convection within the ice based on a Rayleigh number criterion[7], which determines the vertical structure of an effective diffusion $\kappa(z)$ within the ice as a function of depth and is solved using 400 vertical levels, $\partial_z(\kappa(z)\partial_z T) = H(z)/(c_{p,I}\rho_I)$. The tidal heating $H(z)$ is calculated following ref. [9]. The surface ice temperature is calculated using an energy balance between incoming solar radiation, outgoing longwave radiation and internal heating[16,36], assuming a zero heat capacity of the ice and a surface albedo of 0.62 (ref. [24]).

The ice flow model: 'upside-down' shallow ice approximation. We start from the momentum equations in spherical coordinates (longitude, ϕ, co-latitude, θ, and radial, r) when assuming zonal symmetry[37],

$$0 = -\frac{1}{r}\partial_\theta p + \frac{1}{r\sin\theta}\partial_\theta(\sin\theta\tau_{\theta\theta}) + \frac{1}{r^2}\partial_r(r^2\tau_{r\theta}) + \frac{\tau_{r\theta}}{r} - \frac{\cot\theta}{r}\tau_{\phi\phi} \quad (1)$$

and hydrostatic balance

$$\partial_r p = -g\rho_I \quad (2)$$

where p is the pressure, τ_{ij} are the different components of the deviatoric stress tensor, g is the gravity constant and ρ_I is the density of ice (which is assumed to be constant). Since the ice is restricted to a thin layer (~10 km) compared with the radius of Europa[38] (1,561 km), we apply the 'thin-shell' approximation where r is regarded as a constant when it appears by itself. However, variations in the radial direction are important and, to avoid confusion, are denoted by a dependence on a vertical coordinate z; for example, ∂_r is replaced by ∂_z. In the shallow ice approximation, the only stress component that needs to be included is $\tau_{z\theta}$, which is related to the strain rate $\mathring{\epsilon}_{z\theta}$, given by

$$\mathring{\epsilon}_{z\theta} \approx \frac{1}{2}\partial_z v \quad (3)$$

where v is the meridional ice velocity. The derivative along the i direction is indicated by ∂_i while the subscripts of τ and $\mathring{\epsilon}$ indicate the different components of the stress and strain rate tensors. Note that in the seemingly similar problem of Snowball Earth, and unlike here, the global ice flow may be assumed to be independent of depth within the ice[37,39]. In equation (1), only the pressure term and the $\tau_{z\theta}$ term need to be considered in this approximation, as all other terms are much smaller (we verified that these terms are indeed small given the results of our simulations). Then,

$$0 = -\frac{1}{r}\partial_\theta p + \partial_z(\tau_{z\theta}) \quad (4)$$

While ice is a non-Newtonian fluid, generally obeying a nonlinear rheology[40–43], at very small strain rates, it behaves as a Newtonian fluid with a linear rheology, as also used in previous studies of Europa's ice flow[9,17,27,44].

$$\tau_{ij} = \eta(T)\mathring{\epsilon}_{ij}, \quad \eta(T) = \eta_0 \exp\left[\frac{Q_l}{R}\left(\frac{1}{T} - \frac{1}{T_m}\right)\right] \quad (5)$$

where T is the ice temperature, Q_l is the activation energy for diffusive creep, R is the universal gas constant[45], T_m is the melting temperature of ice and η_0 is a constant that quantifies the viscosity of the ice at the melting temperature. For consistency with previous studies[9,27], the melting temperature appearing in the rheology, T_m, is assumed constant—rather than being equal to the freezing temperature T_f calculated from the salinity and pressure (see below). Using a variable T_m yielded very similar results. We have verified that our solution for the ice flow produces stress and strain rates that are in the range appropriate for a linear rheology (Supplementary Fig. 3c,d). Our next objective is to obtain an expression for the ice

velocity. Integrating the hydrostatic equation (2), we find the pressure gradient in terms of the ice thickness,

$$p(z,\theta) = \rho_I g(z_s(\theta) - z)$$

where $z_s(\theta)$ indicates the height of the surface of the ice above sea level. In the standard shallow ice approximation[43], one uses the fact that the stress vanishes at the top of the ice sheet, where it is in contact with air. Here, in our upside-down approximation, we use the fact that the stress vanishes instead at the ice bottom, where it is in contact with water. Substituting in equation (4) this expression for the pressure and integrating from the bottom $z_{b\theta}$ to a level z using the boundary condition at the bottom $\tau_{z\theta}(z_b) = 0$, we find,

$$0 = -\rho_I g(z - z_b)\frac{1}{r}\partial_\theta z_s(\theta) + \tau_{z\theta}(z)$$

Using $\tau_{z\theta} = \eta(T)\mathring{\epsilon}_{z\theta}$ and using the equation (3) for $\mathring{\epsilon}_{z\theta}$, we have

$$0 = -\rho_I g(z - z_b)\frac{1}{r}\partial_\theta z_s + \frac{1}{2}\eta(T)\partial_z v.$$

Next, using $z_s = (1 - \mu)h_I$, $z_b = -\mu h_I$ we find

$$\partial_z v = \frac{2}{r}(1 - \mu)\rho_I g A(T)(z - z_b)\partial_\theta h_I \quad (6)$$

where h_I is the ice thickness, μ is the ratio between the ice density and ocean water density and $A(T) = 1/\eta(T)$. We next obtain the velocity itself by integrating this equation from z to z_{trans}, the depth of the ductile-to-brittle ice transition[46], where the velocity vanishes; z_{trans} is specified at the transition temperature T_{trans} given in Supplementary Table 1. Note again that the standard shallow ice approximation assumes that the velocity vanishes at the bottom of the ice, while here it vanishes at the top of the viscous ice layer, z_{trans}. Another vertical integration now gives the total meridional ice flux,

$$q = \int_{z_b}^{z_{trans}} dz \int_z^{z_{trans}} \partial_{z'} v \; dz' \quad (7)$$

Next, the ice volume conservation equation that relates the total transport q to the ice thickness h_I is

$$\partial_t h_I + \frac{1}{r\sin\theta}\partial_\theta(q\sin\theta) = \frac{1}{\mu}S \quad (8)$$

where $S(\theta)$ is a source term (meters of ocean water per second) due to freezing and melting at the base of the ice, and S/μ represents the rate of change of ice thickness due to the source. This source term is calculated using a heat budget of the ice bottom:

$$L\rho_o S = -\rho_I c_{p,I}\kappa_I \partial_z T \big|_{z_b} - \beta(T_o - T_f) \quad (9)$$

where the first term on the right-hand side is the upward heat flux away from the ice base and the second is the flux into the ice bottom from the ocean, such that $\beta(T_o - T_f) = Q_g$ in the absence of meridional ocean heat transport. The sum of the two, if non-zero, leads to melting or freezing as shown on the left-hand side. In this equation, $T_{o\theta}$ is the ocean temperature (not necessarily equal to the freezing temperature $T_{f\theta}$), L is the latent heat constant of ice, κ_I is the heat conductivity constant of ice, $c_{p,I}$ is the specific heat constant of ice and β is the ocean sensible heat flux coefficient taken from ref. [47].

Temperature within the ice. We solve a diffusion equation for the temperature within the ice,

$$\partial_z(\kappa(z)\partial_z T) = -H(z)/(c_{p,I}\rho_I) \quad (10)$$

where the bottom and top boundary conditions are

$$T(z_b) = T_f(\theta), \; T(z_s) = T_s(\theta)$$

and the tidal heating within the ice is that of equation (13) of ref. [9]:

$$H(z) = \frac{2H_{max}}{\eta/\eta_{max} + \eta_{max}/\eta} \quad (11)$$

Here, $\eta_{max} = \mu_E/\omega$ and $H_{max} = \mu_E \left|\overline{\mathring{\epsilon}_{ij}}\right|^2/\omega$ where μ_E is the elastic shear modulus of ice shell, ω is the rotation rate of Europa and $\left|\overline{\mathring{\epsilon}_{ij}}\right|$ is taken from Fig. 3 of ref. [17] and approximated as $\left|\overline{\mathring{\epsilon}_{ij}}\right| = 2.81072 \times 10^{-10} - 6.823 \times 10^{-11}(1 + \cos(2\phi))^{0.75}$, ϕ being the latitude.

Note that the advection terms are neglected in equation (10) and Supplementary Figs. 4 and 5 show that this is a self-consistent approximation as these terms are indeed much smaller than the diffusion and heat source terms that are used to calculate the temperature—both when convection within the ice is present and when it is absent. The diffusion coefficient $\kappa(z)$ is small and equals to the molecular diffusion in the stagnant layer, but is much larger within the lower convecting layer, representing the efficient heat mixing by convective motions there[9,27,34]. This is represented as follows,

$$\kappa(z) = \kappa_I + (\kappa_{I,c} - \kappa_I)\mathcal{H}(z_{conv} - z)\mathcal{H}(z - (z_b + 2\Delta z_{conv}))$$

$$\mathcal{H}(x) \equiv \frac{1}{2}(\tanh(x/\Delta z_{conv}) + 1)$$

where $\kappa_{I,c}$ is the diffusion coefficient when the ice is convecting and $\mathcal{H}$ is the Heaviside-like step function. The transition depth between the convective and diffusive layers is denoted by z_{conv} and is assumed to be at the depth where the ice temperature is 22 K lower than the freezing temperature (indicating the depth at which the viscosity is approximately one order of magnitude larger than the bottom of the ice melting viscosity[7]). Convection is also assumed to occur only when the thickness of the convective layer yields a Rayleigh number that is larger than a critical Rayleigh number[7,27] $Ra_c = 1,000$; then, $\kappa_{I,c} = 10\kappa_I$ and otherwise $\kappa_{I,c} = \kappa_I$. The Rayleigh number is defined as $Ra = \alpha\rho_I g\Delta T H_{conv}/(\kappa_I\eta_0)$, where α is the thermal expansion coefficient of ice, $\Delta T = 22$ K is the temperature difference over the convective layer, H_{conv} is the thickness of the convecting layer calculated as $z_{conv} - z_b$ and η_0 is the viscosity coefficient at the base of the ice[7,27].

The surface heat flux, which is needed for the calculation of the surface temperature[36], is given by the bottom heat flux plus the integrated internal tidal heating,

$$Q_s = \rho_I c_{p,I}\kappa_I\partial_z T\,|_{z_b} + \int_{z_b}^{z_{conv}} H(z)\,dz$$

The freezing temperature depends on latitude via its dependence on pressure and hence on ice thickness, and via its dependence on salinity, as follows[48], $T_f = A - Bh_I$, where $A = 0.0901 - 0.0575S_o + 273.16$ (S_o being the salinity of the ocean) and $B = 7.61 \times 10^{-8} g\rho_I$ (note that the original expression[48] for T_f is given in degrees Celsius and B multiplies the pressure in dBar, while we converted T_f to degrees Kelvin and reformulated B such that it is multiplied by the ice thickness). In the treatment of the freezing temperature dependence on salinity, we implicitly assumed here that the seawater composition of Europa is similar to that of Earth's ocean, although the actual composition of Europa's ocean is uncertain[32]. The variations of the freezing temperature at the base of the ice due to variations in ice thickness are very small—about a 0.09 K temperature difference for a 1 km difference in ice thickness.

Ocean model. The ocean temperature T_o and heat transport play important roles in determining ice thickness and are calculated here using a simple heat budget equation,

$$\rho_o c_{p,o} h_o\partial_t T_o = Q_g - \beta(T_o - T_f) + \frac{\rho_o c_{p,o}}{r^2\sin\theta}\partial_\theta(h_o\kappa_o\sin\theta\partial_\theta T_o) \quad (12)$$

where $c_{p,o}$ is the specific heat constant of the water and $h_o(\theta) \equiv H_o - \mu(h_I - \langle h_I\rangle)$ is the ocean depth where H_o is the mean ocean depth and $\langle h_I\rangle$ is the latitudinal average of the ice thickness. Meridional heat transport by both eddy mixing and large-scale circulation is parameterized using an eddy mixing coefficient κ_o[25,28–30,49]. Thus, according to equation (12), the rate of ocean heating equals the sum of the internal heating, Q_g, sensible heat flux between the ocean and ice $-\beta(T_o - T_f)$ and lateral ocean transport parameterized as eddy mixing[29,30,50]. The uncertainty in the physics of Europa's ocean heat transport mechanism is sufficiently large that representing it by diffusion and varying the diffusion coefficient over orders of magnitude, as done here, accounts for the necessary wide range of possible transport efficiencies by both ocean circulation and eddies.

Our ocean model formulation is diffusive, does not calculate a circulation and therefore does not rely on a seawater density calculation. The ocean water density, the salinity and pressure dependence of the freezing temperature and other thermodynamic properties of seawater can be calculated using the Gibbs Seawater package[51], which permits self-consistent calculations of the density and other properties of both the fluid and the ice, although one expects the difference from our simpler formulation[48,52] to be small.

Estimates of Europa's ocean salinity vary widely from it being nearly fresh to highly saline[32,53]. To study the sensitivity to the specified mean ocean salinity, S_o, we added a transport equation similar to the one used for the ocean temperature,

$$h_o\partial_t S_o = S\langle S_o\rangle + \frac{1}{r^2\sin\theta}\partial_q(h_o\kappa_o\sin\theta\partial_\theta S_o) \quad (13)$$

where $S(\theta)$ is the source term from equation (9). This equation simply states that local temporal changes in salinity are due to melting and freezing of the ice (the $S\langle S_o\rangle$ term, where $\langle S_o\rangle$ is the meridionally averaged salinity, which in the above

formulation is also constant in time) and meridional salinity transport (the diffusion term). This equation does not take into account brine rejection due to freezing, only salinity changes due to the change of local (positive or negative) input of freshwater[11].

We examined the ice dynamics for a range of prescribed mean ocean salinity values between 0 and 100 ppt and found that the mean ice thickness (Supplementary Fig. 6a) varies by a few hundred meters and the freezing temperature varies by several degrees Kelvin (Supplementary Fig. 6c), yet the ice flow (Supplementary Fig. 6b) is only slightly affected. This dependence on the salinity can be understood as follows. Higher salinity values linearly decrease the freezing temperature[48] by 5.75 K per 100 ppt salinity change (following the freezing temperature equation discussed above). Thus, fresher ocean water leads to a larger temperature difference between the surface of Europa and the ocean, and thus to thicker ice. This difference in ice thickness also affects the freezing temperature due to the pressure effect. In any case, the sensitivity of the thickness to the salinity is not large (of about 30 m per 10 ppt). The ice thickness difference due to changes in the mean freezing temperature can be estimated by $\Delta h_I \approx \kappa_I\rho_I c_{p,I}\Delta T/Q_g$, which yields a ≈ 56.5 m increase in ice thickness for an increase in the freezing temperature of 1 K.

Thus, the model's variables are q, h_I, T_o and S_o and they are solved using equations (7), (8), (12) and (13). These solutions are then used to evaluate the velocity and temperature as functions of latitude and depth in the ice, $v(\theta,z)$, $T(\theta,z)$.

Code availability. The code used for this work is posted on the authors' websites http://www.bgu.ac.il/~ashkena/Europa-ice-flow/ (Y.A.) and http://www.seas.harvard.edu/climate/eli/Downloads/ (E.T.).

Data availability. Data are available from the corresponding author on request.

References

1. Hand, K., Chyba, C., Priscu, J., Carlson, R. & Nealson, K. in *Europa (Space Science Series)* (eds Pappalardo, R. T., McKinnon, W. B. & Khurana, K.) 589–629 (Univ. Arizona Press, Tucson, AZ, 2009).
2. Vance, S., Hand, K. & Pappalardo, R. Geophysical controls of chemical disequilibria in Europa. *Geophys. Res. Lett.* **43**, 4871–4879 (2016).
3. Pappalardo, R. T. et al. Geological evidence for solid-state convection in Europa's ice shell. *Nature* **391**, 365–368 (1998).
4. Kivelson, M. G. et al. Galileo magnetometer measurements: a stronger case for a subsurface ocean at Europa. *Science* **289**, 1340–1343 (2000).
5. Travis, B., Palguta, J. & Schubert, G. A whole-moon thermal history model of Europa: impact of hydrothermal circulation and salt transport. *Icarus* **218**, 1006–1019 (2012).
6. Roth, L. et al. Transient water vapor at Europa's south pole. *Science* **343**, 171–174 (2014).
7. Hussmann, H., Spohn, T. & Wieczerkowski, K. Thermal equilibrium states of Europa's ice shell: implications for internal ocean thickness and surface heat flow. *Icarus* **156**, 143–151 (2002).
8. O'Brien, D. P., Geissler, P. & Greenberg, R. A. A melt through model for chaos formation on Europa. *Icarus* **156**, 152–161 (2002).
9. Tobie, G., Choblet, G. & Sotin, C. Tidally heated convection: constraints on Europa's ice shell thickness. *J. Geophys. Res.* **108**, 5124 (2003).
10. Schenk, P. & Pappalardo, R. T. Topographic variations in chaos on Europa: implications for diapiric formation. *Geophys. Res. Lett.* **31**, L16703 (2004).
11. Zhu, P., Manucharyan, G. E., Thompson, A. F., Goodman, J. C. & Vance, S. D. The influence of meridional ice transport on Europa's ocean stratification and heat content. *Geophys. Res. Lett.* **44**, 5969–5977 (2017).
12. Pappalardo, R. et al. Does Europa have a subsurface ocean? Evaluation of the geological evidence. *J. Geophys. Res.* **104**, 24015–24055 (1999).
13. Collins, G. & Nimmo, F. in *Europa (Space Science Series)* (eds Pappalardo, R. T., McKinnon, W. B. & Khurana, K.) 259–281 (Univ. Arizona Press, Tucson, AZ, 2009).
14. Goodman, J. C., Collins, G. C., Marshall, J. & Pierrehumbert, R. T. Hydrothermal plume dynamics on Europa: implications for chaos formation. *J. Geophys. Res.* **109**, E03008 (2004).
15. Goodman, J. C. & Lenferink, E. Numerical simulations of marine hydrothermal plumes for Europa and other icy worlds. *Icarus* **221**, 970–983 (2012).
16. Ojakangas, G. W. & Stevenson, D. J. Thermal state of an ice shell on Europa. *Icarus* **81**, 220–241 (1989).
17. Nimmo, F., Thomas, P., Pappalardo, R. & Moore, W. The global shape of Europa: constraints on lateral shell thickness variations. *Icarus* **191**, 183–192 (2007).
18. Grasset, O. et al. JUpiter ICy moons Explorer (JUICE): an ESA mission to orbit Ganymede and to characterise the Jupiter system. *Planet. Space Sci.* **78**, 1–21 (2013).

19. Pappalardo, R. et al. Science objectives and capabilities of the NASA Europa mission. In *Lunar and Planetary Science Conf.* **47**, 3058 (Lunar and Planetary Institute, 2016).
20. Billings, S. E. & Kattenhorn, S. A. The great thickness debate: ice shell thickness models for Europa and comparisons with estimates based on flexure at ridges. *Icarus* **177**, 397–412 (2005).
21. Quick, L. C. & Marsh, B. D. Constraining the thickness of Europa's water–ice shell: insights from tidal dissipation and conductive cooling. *Icarus* **253**, 16–24 (2015).
22. Chen, E. M. A., Nimmo, F. & Glatzmaier, G. A. Tidal heating in icy satellite oceans. *Icarus* **229**, 11–30 (2014).
23. Squyres, S. W., Reynolds, R. T., Cassen, P. & Peale, S. J. Liquid water and active resurfacing on Europa. *Nature* **301**, 225–226 (1983).
24. Spencer, J. R., Tamppari, L. K., Martin, T. Z. & Travis, L. D. Temperatures on Europa from Galileo photopolarimeter-radiometer: nighttime thermal anomalies. *Science* **284**, 1514–1516 (1999).
25. Ashkenazy, Y. et al. Dynamics of a Snowball Earth ocean. *Nature* **495**, 90–93 (2013).
26. Hutter, K. *Theoretical Glaciology: Material Science of Ice and the Mechanics of Glaciers and Ice Sheets*. (Reidel, Dordrecht, 1983).
27. Barr, A. C. & Showman, A. P. in *Europa (Space Science Series)* (eds Pappalardo, R. T., McKinnon, W. B. & Khurana, K.) 405–430 (Univ. Arizona Press, Tucson, AZ, 2009).
28. Soderlund, K. M., Schmidt, B. E., Wicht, J. & Blankenship, D. D. Ocean-driven heating of Europa's icy shell at low latitudes. *Nat. Geosci.* **7**, 16–19 (2014).
29. Ashkenazy, Y. & Tziperman, E. Variability, instabilities and eddies in a Snowball ocean. *J. Clim.* **29**, 869–888 (2016).
30. Jansen, M. F. The turbulent circulation of a Snowball Earth ocean. *J. Phys. Oceanogr.* **46**, 1917–1933 (2016).
31. Han, L. & Showman, A. P. Thermo-compositional convection in Europa's icy shell with salinity. *Geophys. Res. Lett.* **32**, L20201 (2005).
32. Zolotov, M. Y. & Kargel, J. in *Europa (Space Science Series)* (eds Pappalardo, R. T., McKinnon, W. B. & Khurana, K.) 431–457 (Univ. Arizona Press, Tucson, AZ, 2009).
33. Sotin, C., Tobie, G., Wahr, J. & McKinnon, W. B. in *Europa (Space Science Series)* (eds Pappalardo, R. T., McKinnon, W. B. & Khurana, K.) 85–117 (Univ. Arizona Press, Tucson, AZ, 2009).
34. Mitri, G. & Showman, A. P. Convective–conductive transitions and sensitivity of a convecting ice shell to perturbations in heat flux and tidal-heating rate: implications for Europa. *Icarus* **177**, 447–460 (2005).
35. Kalousová, K., Schroeder, D. M. & Soderlund, K. M. Radar attenuation in Europa's ice shell: obstacles and opportunities for constraining the shell thickness and its thermal structure. *J. Geophys. Res. Planets* **122**, 524–545 (2017).
36. Ashkenazy, Y. The surface temperature of Europa. Preprint at https://arxiv.org/abs/1608.07372 (2017).
37. Tziperman, E. et al. Continental constriction and sea ice thickness in a Snowball-Earth scenario. *J. Geophys. Res.* **117**, C05016 (2012).
38. Spohn, T., Breuer, D. & Johnson, T. in *Encyclopedia of the Solar System* (eds Prockter, L. M. & Pappalardo, R. T.) Ch. 36 (Elsevier, 2014).
39. Goodman, J. C. & Pierrehumbert, R. T. Glacial flow of floating marine ice in "Snowball Earth". *J. Geophys. Res.* **108**, 3308 (2003).
40. Glen, J. W. The creep of polycrystalline ice. *Proc. R. Soc. Lond. A Math. Phys. Eng. Sci.* **228**, 519–538 (1955).
41. Goldsby, D. & Kohlstedt, D. Superplastic deformation of ice: experimental observations. *J. Geophys. Res.* **106**, 11017–11030 (2001).
42. Durham, W. & Stern, L. Rheological properties of water ice-applications to satellites of the outer planets 1. *Annu. Rev. Earth Planet. Sci.* **29**, 295–330 (2001).
43. Cuffey, K. M. & Paterson, W. S. B. *The Physics of Glaciers* (Academic Press, 2010).
44. Nimmo, F. & Gaidos, E. Strike–slip motion and double ridge formation on Europa. *J. Geophys. Res.* **107**, E4 (2002).
45. Mohr, P. J., Newell, D. B. & Taylor, B. N. Codata recommended values of the fundamental physical constants: 2014. *J. Phys. Chem. Ref. Data* **45**, 043102 (2016).
46. Schulson, E. M. & Duval, P. *Creep and Fracture of Ice* (Cambridge Univ. Press, Cambridge, 2009).
47. Holland, D. M. & Jenkins, A. Modeling thermodynamic ice–ocean interactions at the base of an ice shelf. *J. Phys. Oceanogr.* **29**, 1787–1800 (1999).
48. MITgcm MITgcm User Manual. (MIT/EAPS, Cambridge, MA, 2010); http://mitgcm.org/public/r2_manual/latest/online_documents/manual.html
49. Ashkenazy, Y., Gildor, H., Losch, M. & Tziperman, E. Ocean circulation under globally glaciated Snowball Earth conditions: steady state solutions. *J. Phys. Oceanogr.* **44**, 24–43 (2014).
50. Pollard, D. & Kasting, J. F. Snowball Earth: a thin-ice solution with flowing sea glaciers. *J. Geophys. Res.* **110**, C07010 (2005).
51. McDougall, T. J. & Barker, P. M. *Getting Started With TEOS-10 and the Gibbs Seawater (GSW) Oceanographic Toolbox* (2011).
52. Losch, M. Modeling ice shelf cavities in a *z*-coordinate ocean general circulation model. *J. Geophys. Res.* **113**, C08043 (2008).
53. Hand, K. P. & Chyba, C. F. Empirical constraints on the salinity of the europan ocean and implications for a thin ice shell. *Icarus* **189**, 424–438 (2007).

Acknowledgements

Author contributions

Y.A. and E.T. formulated the problem and performed the model runs and analyses. All authors contributed to the development of the model and the writing of the paper.

Competing interests

The authors declare no competing financial interests.

Additional information

Supplementary information is available for this paper at https://doi.org/10.1038/s41550-017-0326-7.

Reprints and permissions information is available at www.nature.com/reprints.

Correspondence and requests for materials should be addressed to Y.A.

Publisher's note: Springer Nature remains neutral with regard to jurisdictional claims in published maps and institutional affiliations.